

## Article

# Transition Metal Carbides Filler-Reinforced Composite Polymer Electrolyte for Solid-State Lithium-Sulfur Batteries at Room Temperature: Breakthrough

Basem Al Alwan <sup>1,\*</sup>, Zhao Wang <sup>2</sup>, Wissam Fawaz <sup>2</sup> and K. Y. Simon Ng <sup>2</sup><sup>1</sup> Chemical Engineering Department, College of Engineering, King Khalid University, Abha 61411, Saudi Arabia<sup>2</sup> Department of Chemical Engineering and Materials Science, Wayne State University, Detroit, MI 48202, USA

\* Correspondence: beilwan@kku.edu.sa

**Abstract:** All solid-state room-temperature lithium-sulfur (Li-S) batteries have gained increasing attention due to their ability to eliminate the polysulfides shuttle effects and the safety dangers associated with the liquid electrolytes. Herein, a novel composite solid-state electrolyte, which is nickel-tungsten carbides (NiWC) over mesoporous silica (SBA-15) filled polyethylene oxide (PEO), was developed and investigated for Li-S batteries. The filler minimizes the crystallinity of the PEO and increases the ionic conductivity of the electrolyte, resulting in lowering the AC impedance of electrolyte composite from 26,256 ohm to 2416 ohm and to 5734 ohm after adding the electrolyte material with Ni/W ratios of 1:1 and 9:1, respectively. A high initial specific capacity of 1305 mAh g<sup>-1</sup> and a capacity retention of 66.7% after 8 cycles at C/10 was obtained at room temperature after adding NiWC/SBA-15 with a Ni/W ratio of 1:1. This novel composite solid-state electrolyte shows a remarkable long-term performance at high current rates (1, 2, 4, and 5C) and rate capabilities at 0.1, 0.2, 0.5, 1, 2, 4 and back to 0.1C. The battery was able to recover 77% of the initial specific capacity at 0.1C. The materials were characterized by XRD and SEM-EDX to study the crystallinity and elemental distributions, respectively.

**Keywords:** lithium-sulfur batteries; solid-state electrolyte; composite polymer electrolyte; transition metal carbides; polyethylene oxide



**Citation:** Al Alwan, B.; Wang, Z.; Fawaz, W.; Ng, K.Y.S. Transition Metal Carbides Filler-Reinforced Composite Polymer Electrolyte for Solid-State Lithium-Sulfur Batteries at Room Temperature: Breakthrough. *Energies* **2022**, *15*, 7827. <https://doi.org/10.3390/en15217827>

Received: 13 September 2022

Accepted: 20 October 2022

Published: 22 October 2022

**Publisher's Note:** MDPI stays neutral with regard to jurisdictional claims in published maps and institutional affiliations.



**Copyright:** © 2022 by the authors. Licensee MDPI, Basel, Switzerland. This article is an open access article distributed under the terms and conditions of the Creative Commons Attribution (CC BY) license (<https://creativecommons.org/licenses/by/4.0/>).

## 1. Introduction

Lithium-ion batteries have been widely used as energy storage devices for portable electronics, electric vehicles, and power grids [1,2]. However, their low energy density, poor cycle stability, flammable organic liquid electrolytes, and high cost encourage research toward finding better alternatives to avoid these problems. Lithium-sulfur batteries could be the next evolutionary step in the quest for technology beyond the traditional lithium-ion batteries due to their superior properties, such as the theoretical specific capacity of the sulfur electrode of 1672 mAh g<sup>-1</sup> [3–5]. Despite having a high theoretical capacity, their wide usage has been ebbed by some prohibiting shortcomings such as diminished cycle life due to the shuttle effect reaction and the flammability of the organic solvent employed in the electrolyte [6,7]. Many studies have been working on solving the problems mentioned above. Combining carbon materials, such as mesoporous carbon, hollow porous carbon, carbon nanotube, and graphene with sulfur were investigated to improve the sulfur utilization [8–13]. Using solid state electrolytes has been gaining more and more attention to overcome the dendrite formation and shuttling effects of the polysulfides [14–17]. There are four main types of solid electrolytes including gels, solid polymers, inorganic ceramics, and inorganic-organic composite electrolytes. Although inorganic ceramics possess a high ionic conductivity (~10<sup>-3</sup> S cm<sup>-1</sup> at room temperature), they have poor mechanical properties, poor interfacial contact between the solid electrode and the solid electrolyte, and instability in air [18–20]. The ionic conductivity of solid polymer electrolytes is low (~10<sup>-6</sup> S cm<sup>-1</sup> at

room temperature); however, they are more flexible, stretchable, and easier to be fabricated than inorganic ceramics [21].

Several studies have used different approaches to improve the ionic conductivity of polymer electrolytes. It has been concluded that minimizing the crystallinity of polymers could enhance the ionic conductivity of polymer electrolytes [22–24]. Incorporating metal–organic frameworks (MOFs) into the matrix of polymers is a successful approach to improve the ionic conductivity of polymer electrolytes due to the nanoporous structure of MOFs. The nanoporous structure of MOFs provide ideal accommodation for absorbing Li-containing compounds or mixtures in the nanopores that converts it into lithium-ion conductors [25,26]. For instance, a typical MOF material (UIO-66) was added to the poly(ethylene oxide) (PEO) solid electrolyte for lithium-ion battery [27]. A nonvolatile and nonflammable Li-containing ionic liquid (Li-IL), i.e., LiTFSI in 1-ethyl-3-methylimidazolium bis[(trifluoromethyl)sulfonyl]imide [EMIM][TFSI], was added and showed an improvement in the lithium ions transport and cycling stability. In the first cycle, the specific charge capacity of the battery is 151 mAh g<sup>-1</sup> at a rate of 0.5C [27]. The specific discharge capacities of the 10th, 50th, and 100th cycles were measured and found to be 157, 152, and 144 mAh g<sup>-1</sup>, respectively. The efforts of Han et al. studied the use of MOF as a filler for PEO electrolyte in the lithium-ion battery [28]. The battery delivered an initial specific capacity of 144 mAh g<sup>-1</sup> with a high Coulombic efficiency of 98.9%. It has been shown that incorporating a lithium-ion-intercalating material such as lithium cobalt oxide (LCO) could improve the facile transport of lithium ions in the matrix of the active material and the electrolyte [29].

In this work, the ionic conductivity of PEO will be enhanced by reducing its crystallinity and improving the lithium ions transport. To the best of our knowledge, incorporating transition metal carbides supported on mesoporous silica (SBA-15) as a filler in the solid electrolytes for lithium-sulfur batteries has not been investigated. In this study, we propose a new novel composite solid-state electrolyte, which is nickel-tungsten carbides (NiWC) over SBA-15 filled PEO, for lithium-sulfur batteries that can be operated at room temperature. This new composite electrolyte was modified by adding IL and LCO to enhance the capacity and stability of the Li-S battery.

## 2. Materials and Methods

### 2.1. Materials

Poly(ethylene oxide) (PEO, average  $M_v = 300,000$ ), lithium bis(trifluoromethanesulfonyl)imide (LiTFSI, 99.0%), polyvinylidene fluoride (PVDF, average  $M_w = 534,000$ ) were purchased from Aldrich. Anhydrous acetonitrile (HPLC grade) was purchased from EMD Chemicals Inc. Lithium cobalt (III) oxide (LCO, 97.0%) was purchased from Alfa Aesar. N-methyl-2-pyrrolidone (NMP, 99.5%) was purchased from Sigma-Aldrich (St. Louis, MI, USA).

### 2.2. Preparation of the NiWC/SBA-15-IL

NiWC/SBA-15 with different Ni/W ratios (9:1, and 1:1) were prepared by impregnation method as reported previously [30]; 1-butyl-3-methylimidazolium bis(trifluoromethylsulfonyl imide) [BMIMTFSI], and N-butyl-N-methylpyrrolidinium bis(trifluoromethanesulfonyl) imide [PYR14TFSI] were prepared and used as room-temperature ionic liquids as described previously [31]. The prepared NiWC/SBA-15 was mixed with the prepared ionic liquid with a weight ratio of 3:4, and then heated at 120 °C under a vacuum for 12 h to obtain the NiWC/SBA-15-IL.

### 2.3. Preparation of the Solid Electrolyte (PEO-LiTFSI-NiWC/SBA-15-IL-LCO)

PEO was dried at 50 °C, and LiTFSI was dried at 100 °C for 24 h under vacuum and stored in an Ar-filled glove box. Then, 1.0 g PEO was mixed with 0.4 g LiTFSI, dissolved in 30 mL acetonitrile, and magnetically stirred at 60 °C for 2 h. The LCO was added to the mixture with a weight ratio of 60:40. A 30 wt% of the nanostructured NiWC/SBA-15-IL

was added to the mixture, and then sonicated for 10 min to get a homogeneous solution. Finally, the solution was magnetically stirred at 60 °C for 24 h.

#### 2.4. Preparation of the Cathode (S-CoS@CNT-PEO-LiTFSI-NiWC/SBA-15-IL-LCO)

The cathode electrode slurry was prepared by melt-diffusion method of sulfur with 20%-CoS@multi-wall carbon nanotubes (CoS@MWCNT) with a weight ratio of 70 wt% to 30 wt% as reported previously [32]. The mixture was mixed with Super P with a weight ratio of 72:28. PVDF and LCO were added to the mixture with a weight ratio of the mixture, PVDF, and LCO as 60, 33, and 7, respectively. The prepared PEO-LiTFSI-NiWC/SBA-15-IL was added to the mixture with a weight ratio of 40 to 60. An adequate amount of NMP was added to the mixture as a solvent to form a slurry. After grinding the slurry for 90 min, the slurry was coated on aluminum foil by the doctor blade, and then dried at 60 °C under vacuum for 6 h.

#### 2.5. Materials Characterization

X-ray Diffraction (XRD) patterns of the materials were acquired by a Bruker D2 Phaser using Cu K $\alpha$  radiation at room temperature to analyze the crystallinity of the materials at angles from 10 to 80°. The elemental distribution on the cathode and electrolyte were characterized by the Field-Emission Scanning Electron Microscopy (JSM-7600 FE SEM).

#### 2.6. The Assembly of the Cells

The cathode surface was directly coated by the solid polymer electrolyte slurry using the doctor blade to minimize the interfacial resistance between the cathode and the electrolyte. The cathode/electrolyte material was dried at 60 °C under vacuum for 6 h. The cathode-electrolyte material and lithium were cut with diameters of 14 mm and 12 mm, respectively. The cells were made using LIR2032 coin cells. All cells were assembled in an Ar-filled glovebox ( $O_2 < 0.1$  ppm,  $H_2O < 0.1$  ppm).

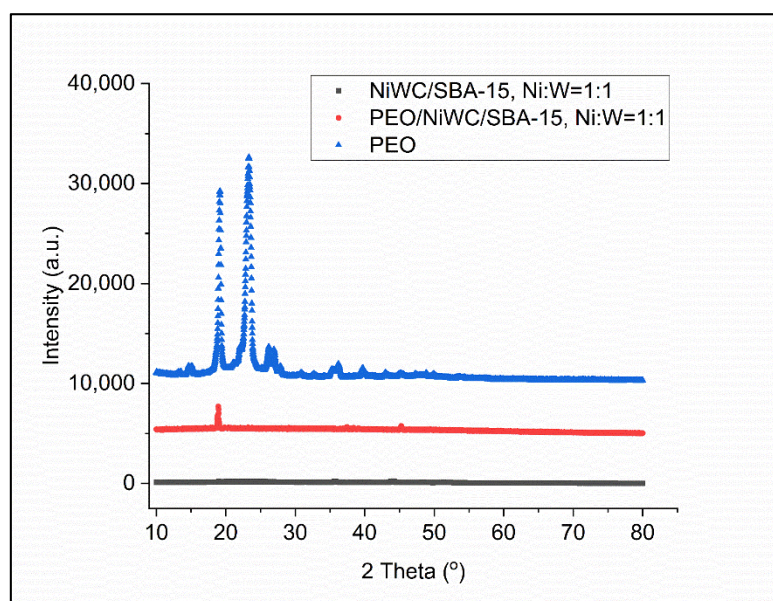
#### 2.7. Electrochemical Measurements

Galvanostatic discharge-charge tests were conducted by Maccor Model 4200 Automated Test System between a voltage range of 1.5–3.0 V (vs. Li/Li<sup>+</sup>) at room temperature. The electrochemical impedance spectroscopy (EIS) and cyclic voltammetry (CV) experiments were tested by using a CH Instruments CHI660D Electrochemical Workstation. The scan rate of CV is 0.1 mV/s and the frequency of EIS is from 0.1 to 1,000,000 Hz.

### 3. Results

#### 3.1. Materials Crystallography

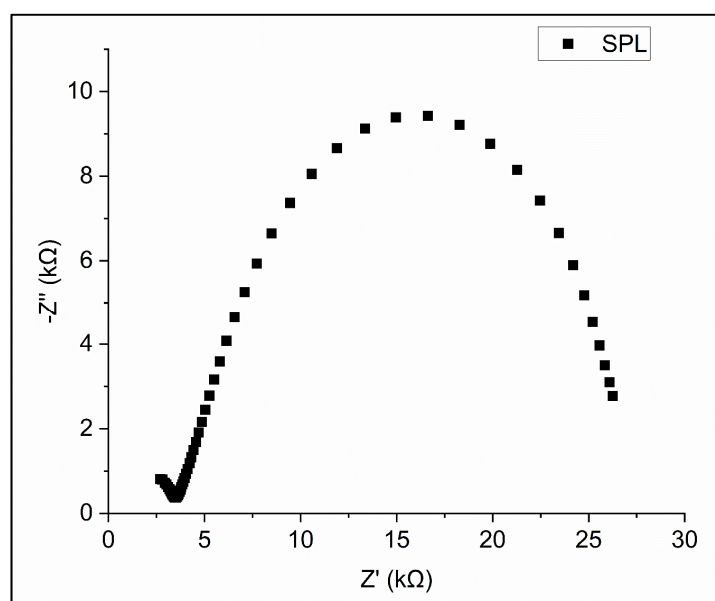
Figure 1 shows the XRD patterns of the PEO, NiWC/SBA-15 (Ni/W = 1:1), and PEO/NiWC/SBA-15 (Ni/W = 1:1). The XRD pattern of the PEO has two prominent peaks at 19.1° and 23.3°, indicating that the PEO has high level of crystalline structure [33]. The XRD pattern of the NiWC/SBA-15 (Ni/W = 1:1) shows an amorphous structure due to the existence of SBA-15. The intensities of the peaks of PEO become weaker after adding the NiWC/SBA-15 (Ni/W = 1:1), suggesting that the degree of crystallization of PEO could be lowered by the addition of NiWC/SBA-15 (Ni/W = 1:1). Therefore, the segmental motion of the polymer chains of PEO could be increased, which leads to an increase in the ionic conductivity [31].



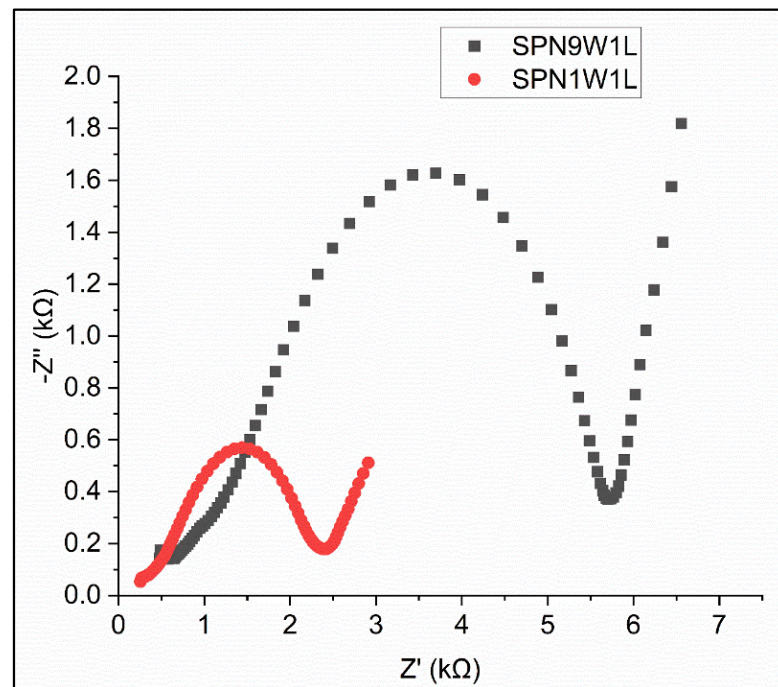
**Figure 1.** XRD patterns of the PEO, NiWC/SBA-15 (Ni/W = 1:1), and PEO/NiWC/SBA-15 (Ni/W = 1:1).

### 3.2. The Electrochemical Performance

The EIS measurements shown in Figure 2 illustrate the impedance for S-CoS@CNT-PEO-LiTFSI-LCO/PEO-LiTFSI-LCO/Li metal (SPL) cell, and Figure 3 presents the impedance for both S-CoS@CNT-PEO-LiTFSI-NiWC/SBA-15-IL-LCO/PEO-LiTFSI-NiWC/SBA-15-IL-LCO/Li metal (SPN1W1L) with a ratio of Ni/W = 1:1 and SPN9W1L with a ratio of Ni/W = 9:1 cells before cycling. A significant reduction in the impedance were occurred after incorporating the NiWC/SBA-15-IL and LCO into the matrix of the electrolyte and the cathode. The impedance was lowered from 26,256 ohm to 2416 ohm and to 5734 ohm after adding the electrolyte material with Ni/W = 1:1 and with Ni/W = 9:1, respectively. This suggests that the amorphous structure of NiWC/SBA-15 provides accommodation for absorbing Li-containing compounds in the nanopores that makes it a better lithium-ion conductor [25,26]. Moreover, the addition of LCO promotes the movement of lithium ions in the cathode and the electrolyte [29].

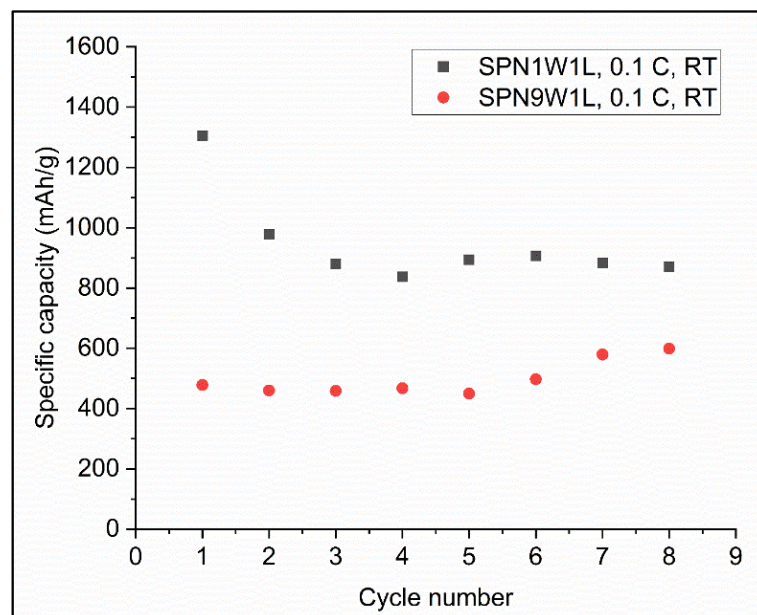


**Figure 2.** Nyquist plots of the S-CoS@CNT-PEO-LiTFSI-LCO/PEO-LiTFSI-LCO/Li metal.



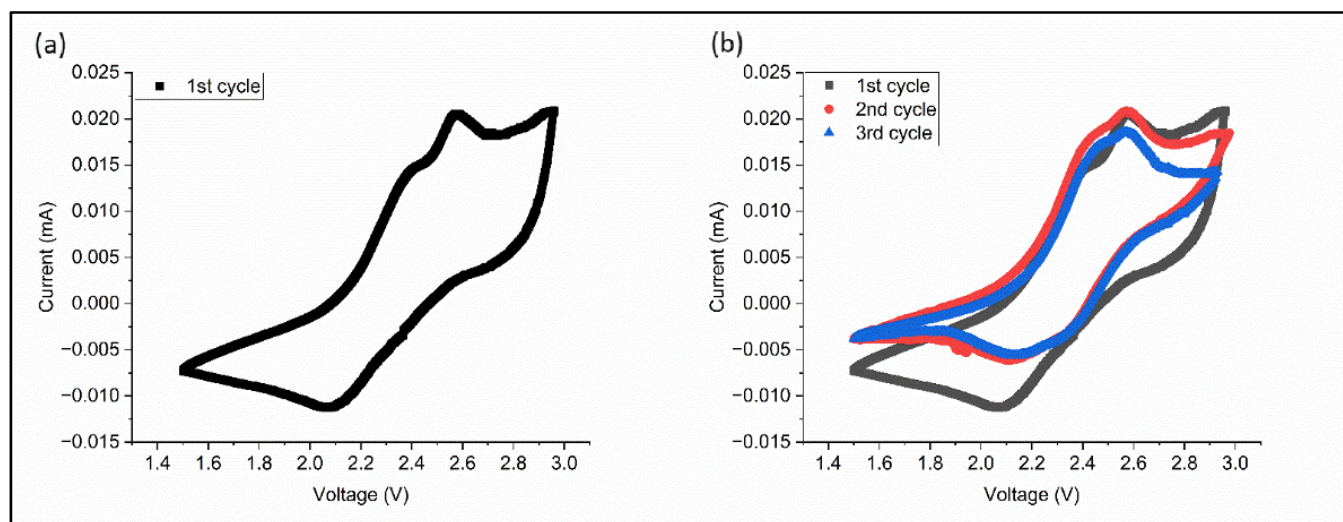
**Figure 3.** Nyquist plots of the SPNWL, Ni/W = 1:1 and the SPNWL, Ni/W = 9:1.

Figure 4 shows the specific capacities at room temperature in a voltage window of 1.5–3.0 V at a rate of C/10 for both SPN1W1L and SPN1W9L cells. The initial specific capacity of  $1305 \text{ mAh g}^{-1}$  and  $478 \text{ mAh g}^{-1}$  was obtained for SPN1W1L and SPN1W9L, respectively. The specific capacity of SPN1W1L leveled off after the third cycle with a capacity retention of 66.7% after eight cycles. This compared favorably to the best reported finding for Li-S polymer-electrolyte-system with an initial energy capacity of around  $1481 \text{ mAh g}^{-1}$ , and a capacity retention of approximately 60.0% after eight cycles at a lower current rate of C/20 [29].



**Figure 4.** Specific capacity vs. cycle number of the SPNWL, Ni/W = 1:1 and the SPNWL, Ni/W = 9:1. The cells were operated under C/10 at room temperature.

The SPN1W1L cell was further investigated to study the electrochemical performance. Cyclic voltammograms have been recorded in the voltage range of 1.5–3.0 V at a scan rate of 0.1 mV/s. Figure 5a shows peaks around 2.1 V and 2.5 V in the first scan which are attributed to the reduction of sulfur to lithium polysulfides ( $\text{Li}_2\text{S}_n$ ,  $2 < n < 8$ ) and oxidation of lithium sulfides to elemental sulfur and lithium, respectively [34,35]. During the second cycle of the voltammetry, and onwards (Figure 5b), there were no significant changes in the reduction and oxidation peaks. The anodic peak area is smaller than that of the cathodic peak due to the high sweeping rate applied for the experiments, as the rate of mass transfer of  $\text{Li}^+$  to S and polysulfides is higher than that of the rate of electron transfer [36].



**Figure 5.** Cyclic voltammogram of the SPNWL, Ni/W = 1:1 battery at a scan rate of 0.1 mV/s. (a) First cycle. (b) First, second, and third cycles.

Figure 6 shows the discharge capacities of the SPN1W1L cell were measured at different current rates (1, 2, 4, and 5C) at room temperature for over 100 cycles. High initial discharge capacities of 526, 485, 190, and 174  $\text{mAh g}^{-1}$  were obtained at 1, 2, 4, and 5C, respectively. However, the specific capacities started decreasing due to several reasons. Firstly, the capacity fading can be partly attributed to the increase bulk resistances as indicated by the second semicircles in the EIS spectra (Figure 7) after 100 cycles at 2, 4, and 5C [37]. Moreover, the bulk resistances were increased to 8.3 k, 11.2 k, and 12.1 k after running the batteries at 2, 4, and 5C, respectively. Secondly, the SEM and EDX mapping (Figure 8) shows the migration of W from the solid electrolyte toward the cathode side that might contributing to the increase in electrolyte resistance. Figure 8a shows that the S, Ni, and W were very well dispersed over the cathode and the electrolyte before cycling. However, the distribution of Ni and W were largely disturbed after 100 cycles at 2C. The migration of Ni and W particles lowers the content of the transition metal fillers in the electrolyte which causes lowering the ionic conductivity of the electrolyte; therefore, decreasing the specific capacities of the batteries. Finally, the volume expansion occurs during the discharge of the cathode where sulfur is converted to lithium disulfide could disturb the solid electrolyte structure and have an effect on lowering the specific capacity of the batteries [29]. The average coulombic efficiency is about 92%, while the capacity retentions after 100 charge-discharge cycles were 34, 5, 4, and 4% at 1, 2, 4, and 5C, respectively.

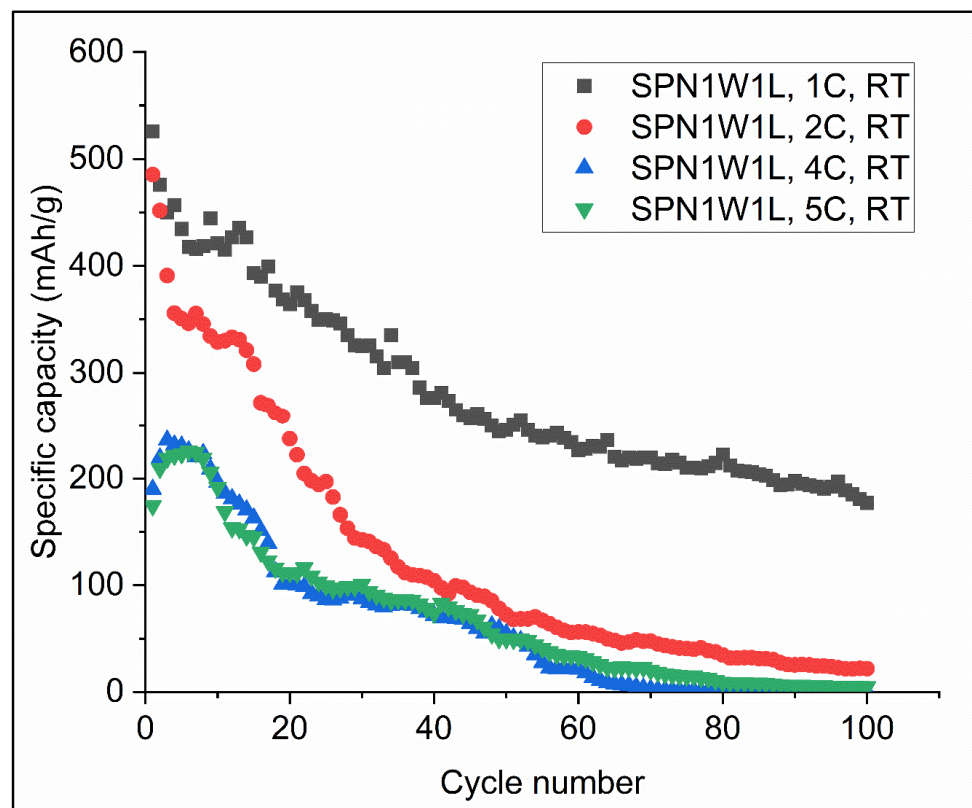


Figure 6. Cyclic performance of the SPNWL, Ni/W = 1:1 batteries at 1C, 2C, 4C, and 5C.

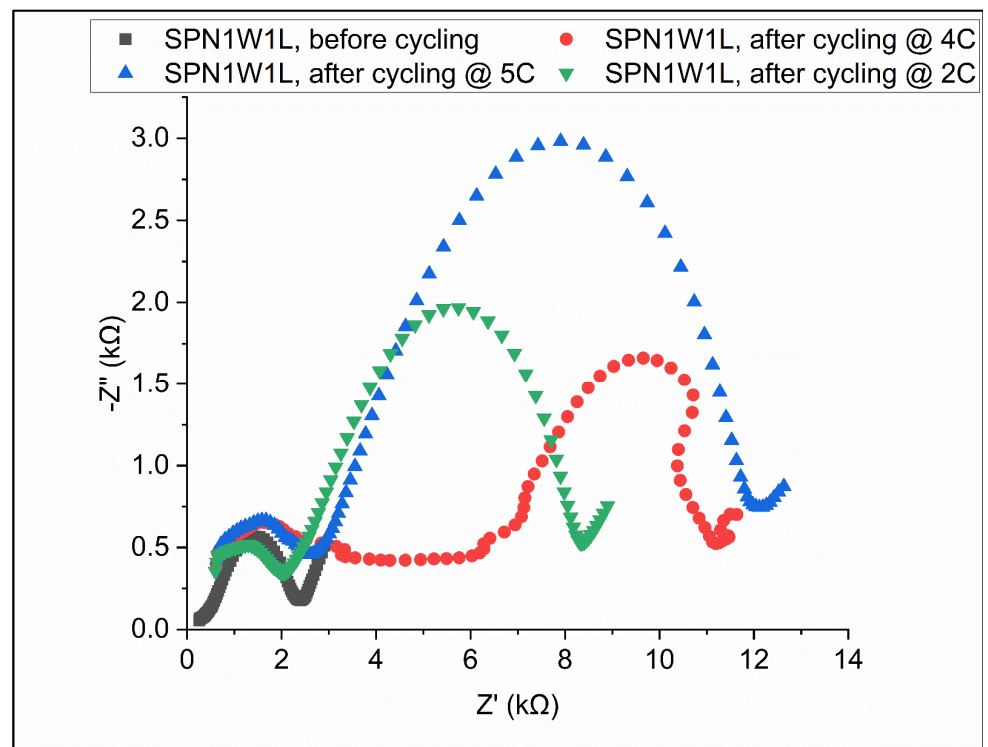
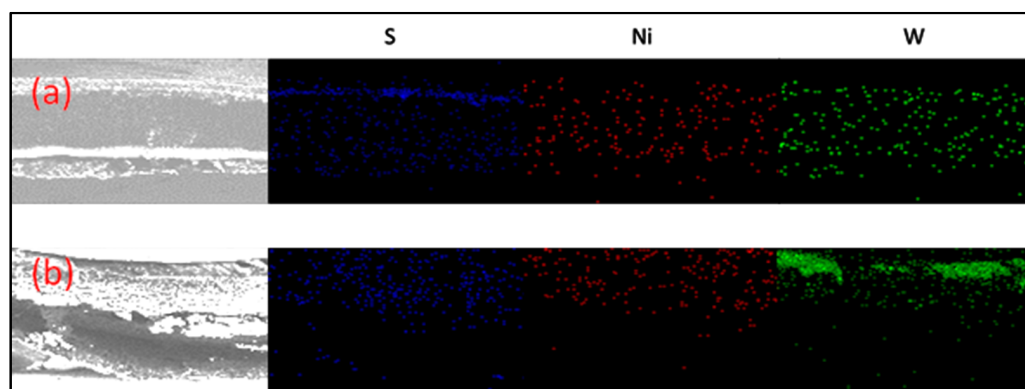
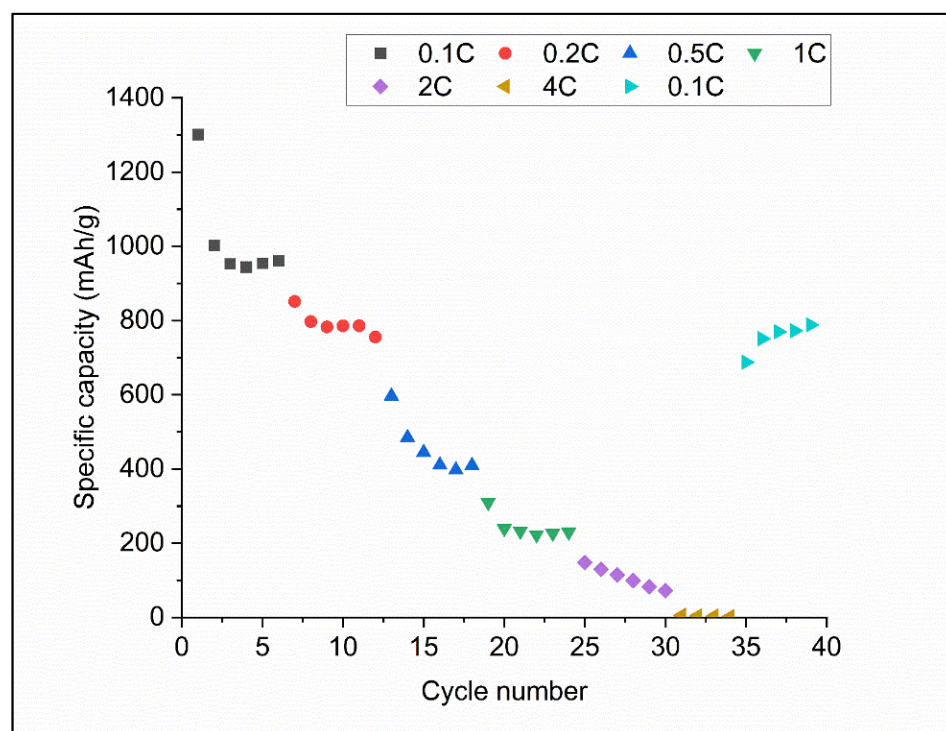


Figure 7. AC impedance spectra of the SPNWL, Ni/W = 1:1 batteries before cycling, after 100 cycles at 2C, 4C, and 5C.



**Figure 8.** SEM and EDX mapping for S, Ni, and W of the SPNWL, Ni/W = 1:1 batteries (a) before cycling; (b) after 100 cycles at 2C.

The rate capability of SPN1W1L was investigated by cycling at charge-discharge rates varying from 0.1C to 4C with cutoff voltages of 1.5 and 3.0 V (Figure 9). Although the capacity dropped significantly at a high C-rate of 4C, 77% of the 0.1C capacity was recovered when lowering the rate again to 0.1C. These results suggest that the sulfur utilization was impeded at high C-rate; therefore, the sulfur electrode polarization is an important issue to address [38]. The recovering of 77% of the capacity after lowering the discharge rate highlights the good performance of the all-solid-state Li-S battery SPN1W1L.



**Figure 9.** Rate capability of the SPNWL, Ni/W = 1:1 battery at 0.1, 0.2, 0.5, 1, 2, and 4 C-rates.

In this study, it has been demonstrated that the addition of transition metal carbides supported on mesoporous silica (NiWC/SBA-15) reduces the crystallinity of the PEO due to the amorphous structure of the SBA-15, and increases the ionic conductivity of the solid electrolyte due to the high conductivity of the metal carbide phase [39]. Moreover, this study indicated that the existence of LCO and IL are essential to provide a facile transport of lithium ions in the matrix of the electrolyte [29] and to increase the ionic conductivity of the electrolyte [31], respectively. Compared to the previous studies, Elizalde-Segovia et al. [29] utilized the LCO as a second layer in the solid electrolyte without adding the transition

metal carbides in Li-S battery. The Li-S cells delivered an initial specific capacity of around 1481 mAh g<sup>-1</sup>, and a capacity retention of approximately 60.0% after eight cycles, but at a lower current rate of C/20 [29]; however, the long-term performance of the battery was not investigated and only eight cycles were reported. This study shows that the SPN1W1L not only can achieve a high initial specific capacity of 1305 mAh g<sup>-1</sup> and better capacity retention of 66.7% after eight cycles at a higher current rate of C/10, but also shows a longer-term performance with higher current rates, and good rate capability.

#### 4. Conclusions

This is the first study of transition metal carbides supported on mesoporous silica (NiWC/SBA-15) as a filler in the solid composite polymer electrolyte for Li-S batteries. The addition of NiWC/SBA-15 reduced the resistance of the all-solid-state Li-S battery due to the existence of amorphous structure of SBA-15 and the high conductivity of the NiW carbide phase. The results were a breakthrough in terms of initial specific conductivity, rate capability, and long-term performance. The initial specific capacity and capacity retention of SPN1W1L were 1305 mAh g<sup>-1</sup> and 66.7% after eight cycles, respectively. Moreover, it shows great potential to perform at high rates (1, 2, 4, and 5C) and shows the ability to accommodate the changing in current rates in the order of 0.1, 0.2, 0.5, 1, 2, 4, then 0.1C, as well as regaining 77% of the initial specific capacity. Using transition metal carbides supported on mesoporous silica is a novel and promising approach. Further investigations, such as stabilizing the TMC within the PEO matrix, and the effect of mono- and tri-transition metal carbides on the performance of Li-S batteries should be made.

**Author Contributions:** Conceptualization, B.A.A. and K.Y.S.N.; formal analysis, B.A.A. and K.Y.S.N.; funding acquisition, B.A.A. and K.Y.S.N.; investigation, B.A.A. and Z.W.; methodology, B.A.A., Z.W. and W.F.; supervision, B.A.A. and K.Y.S.N.; validation, B.A.A., Z.W. and W.F.; writing—original draft, B.A.A.; writing—review & editing, K.Y.S.N. All authors have read and agreed to the published version of the manuscript.

**Funding:** This study was funded by Deanship of Scientific Research (Project No.: RGP2/214/43), King Khalid University, Abha, K.S.A.

**Acknowledgments:** The research work was funded by the Deanship of scientific Research, Saudi Arabia (Project NO.: RGP2/214/43), King Khalid University Abha, K.S.A. The author Basem Al Alwan, therefore, acknowledge with thanks to DSR and the Chemical Engineering Department in the College of Engineering (KKU) for financial and technical support.

**Conflicts of Interest:** The authors declare that they have no conflict of interest.

#### References

1. Armand, M.; Tarascon, J.M. Building better batteries. *Nature* **2008**, *451*, 652–657. [[CrossRef](#)] [[PubMed](#)]
2. Goodenough, J.B.; Park, K.S. The Li-Ion Rechargeable Battery: A Perspective. *J. Am. Chem. Soc.* **2013**, *135*, 1167–1176. [[CrossRef](#)] [[PubMed](#)]
3. Huang, L.; Liu, B.; Li, Y.H.; Shen, S.H.; Deng, S.J.; Wang, X.L.; Xia, X.H.; Tu, J.P. Electrode Design for Lithium–Sulfur Batteries: Problems and Solutions. *Adv. Funct. Mater.* **2020**, *30*, 1910375. [[CrossRef](#)]
4. Chen, X.; Hou, T.; Persson, K.A.; Zhang, Q. Combining theory and experiment in lithium–sulfur batteries: Current progress and future perspectives. *Mater. Today* **2019**, *22*, 142–158. [[CrossRef](#)]
5. Zhao, H.; Deng, N.; Yan, J.; Kang, W.; Ju, J.; Ruan, Y.; Wang, X.; Zhuang, X.; Li, Q.; Cheng, B. A review on anode for lithium-sulfur batteries: Progress and prospects. *Chem. Eng. J.* **2018**, *347*, 343–365. [[CrossRef](#)]
6. Fotouhi, A.; Auger, D.; O'Neill, L.; Cleaver, T.; Walus, S. Lithium-Sulfur Battery Technology Readiness and Applications—A Review. *Energies* **2017**, *10*, 1937. [[CrossRef](#)]
7. Rong, G.; Zhang, X.; Qiu, Y.; Liu, M.; Ye, F.; Xu, Y.; Chen, J.; Hou, Y.; Li, W.; Zhang, Y. Liquid-Phase Electrochemical Scanning Electron Microscopy for In Situ Investigation of Lithium Dendrite Growth and Dissolution. *Adv. Mater.* **2017**, *29*, 1606187. [[CrossRef](#)]
8. Ji, X.; Lee, K.T.; Nazar, L.F. A highly ordered nanostructured carbonsulphur cathode for lithium-sulphur batteries. *Nat. Mater.* **2009**, *8*, 500–506. [[CrossRef](#)]
9. Jayaprakash, N.; Shen, J.; Moganty, S.S.; Corona, A.; Archer, L.A. Porous hollow carbon@sulfur composites for high-power lithium-sulfur batteries. *Angew Chem. Int. Ed.* **2011**, *50*, 5904–5908. [[CrossRef](#)] [[PubMed](#)]

10. Guo, J.; Xu, Y.; Wang, C. Sulfur-impregnated disordered carbon nanotubes cathode for lithium-sulfur batteries. *Nano Lett.* **2011**, *11*, 4288–4294. [[CrossRef](#)]
11. Zhang, J.; Zheng, C.; Lou, J.; Xia, Y.; Liang, C.; Huang, H.; Gan, Y.; Tao, X.; Zhang, W. Poly(ethylene oxide) reinforced  $\text{Li}_6\text{PS}_5\text{Cl}$  composite solid electrolyte for all-solid-state lithium battery: Enhanced electrochemical performance, mechanical property and interfacial stability. *J. Power Sources* **2019**, *412*, 78–85. [[CrossRef](#)]
12. Wang, H.; Yang, Y.; Liang, Y.; Robinson, J.T.; Li, Y.; Jackson, A.; Cui, Y.; Dai, H. Graphene-wrapped sulfur particles as a rechargeable lithium-sulfur battery cathode material with high capacity and cycling stability. *Nano Lett.* **2011**, *11*, 2644–2647. [[CrossRef](#)] [[PubMed](#)]
13. Liu, C.; Bai, Y.; Zhao, Y.; Yao, H.; Pang, H.  $\text{MoS}_2$ /graphene composites: Fabrication and electrochemical energy storage. *Energy Storage Mater.* **2020**, *33*, 470–502. [[CrossRef](#)]
14. Judez, X.; Zhang, H.; Li, C.; Eshetu, G.G.; González-Marcos, J.A.; Armand, M.; Rodríguez-Martinez, L.M. Review—Solid Electrolytes for Safe and High Energy Density Lithium-Sulfur Batteries: Promises and Challenges. *J. Electrochem. Soc.* **2018**, *165*, A6008–A6016. [[CrossRef](#)]
15. Manthiram, A.; Yu, X.; Wang, S. Lithium battery chemistries enabled by solid-state electrolytes. *Nat. Rev. Mater.* **2017**, *2*, 16103. [[CrossRef](#)]
16. Lin, Z.; Liang, C. Lithium-sulfur batteries: From liquid to solid cells. *J. Mater. Chem. A* **2015**, *3*, 936. [[CrossRef](#)]
17. Umeshbabu, E.; Zheng, B.; Yang, Y. Recent Progress in All-Solid-State Lithium-Sulfur Batteries Using High Li-Ion Conductive Solid Electrolytes. *Electrochem. Energ. Rev.* **2019**, *2*, 199. [[CrossRef](#)]
18. Wang, Y.; Sahadeo, E.; Rubloff, G.; Lin, C.F.; Lee, S.B. High-capacity lithium sulfur battery and beyond: A review of metal anode protection layers and perspective of solid-state electrolytes. *J. Mater. Sci.* **2019**, *54*, 3671. [[CrossRef](#)]
19. Sun, Y.Z.; Huang, J.Q.; Zhao, C.Z.; Zhang, Q. A review of solid electrolytes for safe lithium-sulfur batteries. *Sci. China Chem.* **2017**, *60*, 1508–1526. [[CrossRef](#)]
20. Bachman, J.C.; Muy, S.; Grimaud, A.; Chang, H.H.; Pour, N.; Lux, S.F.; Paschos, O.; Maglia, F.; Lupart, S.; Lamp, P.; et al. Inorganic Solid-State Electrolytes for Lithium Batteries: Mechanisms and Properties Governing Ion Conduction. *Chem. Rev.* **2016**, *116*, 140–162. [[CrossRef](#)]
21. Zhang, Q.; Liu, K.; Ding, F.; Liu, X. Recent advances in solid polymer electrolytes for lithium batteries. *Nano Res.* **2017**, *10*, 4139–4174. [[CrossRef](#)]
22. Zhang, D.; Zhang, L.; Yang, K.; Wang, H.; Yu, C.; Xu, D.; Xu, B.; Wang, L.M. Superior Blends Solid Polymer Electrolyte with Integrated Hierarchical Architectures for All-Solid-State Lithium-Ion Batteries. *ACS Appl. Mater. Interfaces* **2017**, *9*, 36886–36896. [[CrossRef](#)]
23. Puthirath, A.B.; Patra, S.; Pal, S.; Manoj, M.; Puthirath Balan, A.; Jayalekshmi, S.; Tharangattu, N.N. Transparent flexible lithium ion conducting solid polymer electrolyte. *J. Mater. Chem. A* **2017**, *5*, 11152–11162. [[CrossRef](#)]
24. Zhang, J.; Zang, X.; Wen, H.; Dong, T.; Chai, J.; Li, Y.; Chen, B.; Zhao, J.; Dong, S.; Ma, J.; et al. High-voltage and free-standing poly(propylene carbonate)/ $\text{Li}_{6.75}\text{La}_3\text{Zr}_{1.75}\text{Ta}_{0.25}\text{O}_{12}$  composite solid electrolyte for wide temperature range and flexible solid lithium ion battery. *J. Mater. Chem. A* **2017**, *5*, 4940–4948. [[CrossRef](#)]
25. Sun, L.; Park, S.S.; Sheberla, D.; Dinca, M. Measuring and Reporting Electrical Conductivity in Metal-Organic Frameworks:  $\text{Cd}_2(\text{TTFTB})$  as a Case Study. *J. Am. Chem. Soc.* **2016**, *138*, 14772–14782. [[CrossRef](#)]
26. Park, S.S.; Tulchinsky, Y.; Dinca, M. Single-Ion  $\text{Li}^+$ ,  $\text{Na}^+$ , and  $\text{Mg}^{2+}$  Solid Electrolytes Supported by a Mesoporous Anionic Cu-Azolate Metal-Organic Framework. *J. Am. Chem. Soc.* **2017**, *139*, 13260–13263. [[CrossRef](#)]
27. Wu, J.; Guo, X. MOF-derived nanoporous multifunctional fillers enhancing the performances of polymer electrolytes for solid-state lithium batteries. *J. Mater. Chem. A* **2019**, *7*, 2653–2659. [[CrossRef](#)]
28. Han, X.; Wu, T.; Gu, L.; Tian, D. A Li-based MOF-derived multifunctional PEO polymer solid-state electrolyte for lithium energy storage. *New J. Chem.* **2022**, *46*, 3747–3753. [[CrossRef](#)]
29. Elizalde-Segovia, R.; Irshad, A.; Zayat, B.; Narayanan, S.R. Solid-State Lithium-Sulfur Battery Based on Composite Electrode and Bi-layer Solid Electrolyte Operable at Room Temperature. *J. Electrochem. Soc.* **2020**, *167*, 140529. [[CrossRef](#)]
30. Al Alwan, B.; Sari, E.; Salley, S.O.; Ng, K.Y.S. Effect of Metal Ratio and Preparation Method on Nickel-Tungsten Carbide Catalyst for Hydrocracking of Distillers Dried Grains with Solubles Corn Oil. *Ind. Eng. Chem. Res.* **2014**, *53*, 6923–6933. [[CrossRef](#)]
31. Ara, M.; Meng, T.; Nazri, G.; Salley, S.O.; Ng, K.Y.S. Ternary Imidazolium-Pyrrolidinium-Based Ionic Liquid Electrolytes for Rechargeable Li-O<sub>2</sub> Batteries. *J. Electrochem. Soc.* **2014**, *161*, A1–A7. [[CrossRef](#)]
32. Wang, Z.; Zeng, W.; Ng, K.Y.S. Facile Synthesis of CoS Nanoparticles Anchored on the Surface of Functionalized Multiwalled Carbon Nanotubes as Cathode Materials for Advanced Li-S Batteries. *Ind. Eng. Chem. Res.* **2022**, *61*, 9322–9330. [[CrossRef](#)]
33. Ge, Z.; Li, J.; Liu, J. Enhanced electrochemical performance of all-solid-state sodium-sulfur batteries by PEO- $\text{NaCF}_3\text{SO}_3$ -MIL-53(Al) solid electrolyte. *Ionics* **2020**, *26*, 1787–1795. [[CrossRef](#)]
34. Kumaresan, K.; Mikhaylik, Y.; White, R.E. A Mathematical Model for a Lithium-Sulfur Cell. *J. Electrochem. Soc.* **2008**, *155*, A576–A582. [[CrossRef](#)]
35. Barchasz, C.; Molton, F.; Duboc, C. Lithium/sulfur cell discharge mechanism: An original approach for intermediate species identification. *Anal. Chem.* **2012**, *84*, 3973–3980. [[CrossRef](#)]
36. Pletcher, D.; Greff, R.; Peat, R.; Peter, L.M.; Robinson, J. *Instrumental Methods in Electrochemistry*, 1st ed.; Woodhead Publishing: Philadelphia, PA, USA, 2001; p. 442.

37. Mei, B.; Lau, J.; Lin, T.; Tolbert, S.H.; Dunn, B.S.; Pilon, L. Physical Interpretations of Electrochemical Impedance Spectroscopy of Redox Active Electrodes for Electrical Energy Storage. *J. Phys. Chem. C* **2018**, *122*, 24499–24511. [[CrossRef](#)]
38. Das, S.; Ngene, P.; Norby, P.; Vegge, T.; Jongh, P.; Blanchard, D. All-Solid-State Lithium-Sulfur Battery Based on a Nanoconfined  $\text{LiBH}_4$  Electrolyte. *J. Electrochem. Soc.* **2016**, *163*, A2029–A2034. [[CrossRef](#)]
39. Zhong, Y.; Xia, X.; Shi, F.; Zhan, J.; Tu, J.; Fan, H.J. Transition Metal Carbides and Nitrides in Energy Storage and Conversion. *Adv. Sci.* **2016**, *3*, 1500286. [[CrossRef](#)]